Free Vibration of Thick FGM Plates under TSDT and Thermal Environment

Chih-Chiang Hong[*]

Department of Mechanical Engineering, Hsiuping University of Science and Technology, Taichung, Taiwan

Abstract

Three parameters of thermal environment, varied calculated shear correction, and third-order shear deformation theory (TSDT) of displacement are important in the frequency study. These three effects have been studied on the non-dimensional and dimensional frequencies of thick FGM plates. An additional c_1 displacement term in nonlinear coefficient of TSDT is used to present the frequency of vibration into the simply homogeneous equation of thick FGM plates. The determinant of the coefficient matrix containing the c_1 displacement term in dynamic differential equilibrium equations can be derived into the five degree polynomial free vibration equation. The non-dimensional and dimensional of natural frequency can be obtained. The effects of plate thickness, temperature of environment and power law index of FGM on the non-dimensional and dimensional frequency of FGM plates are investigated.

Keywords: TSDT, FGM, frequency, nonlinear, homogeneous

1. Introduction

Recently, many vibration papers devoted to the studies of mechanics of homogeneous, functionally graded material (FGM) porous beams/plates at micro, macro and nanoscales, diverse plates/beams theories, and linear/nonlinear thickness changes. In 2020, Żur et al. [1] presented the free vibration by using the nonlocal sinusoidal higher-order shear deformation theory (HSDT) for the magneto-electro-elastic FGM nanoplates. In 2020, Ouakad et al. [2] presented the nonlinear vibration by using the stress-driven nonlocal integral elasticity for the actuated hybrid nanotubes. In 2020, Ghobadi et al. [3] presented the nonlinear free vibration by using the Galerkin's and perturbation methods for the FGM flexoelectric nano-plates. In 2020, Ghobadi et al. [4] presented the nonlinear vibration by using the Galerkin's and multiple scale methods for the FGM thermo-electro-elastic nanostructures. In 2021, Guo et al. [5] presented the non-dimensional frequency by using the element-free IMLS-Ritz method for the graphene nanoplatelets reinforced composite (GPLRC) plates with matrix cracks.

There are some non-dimensional and dimensional frequency of vibration presentations in the composite structure of plates. In 2020, Babaei et al. [6] used the 3D elasticity theory of structures to investigate the non-dimensional natural frequency of saturated porous annular sector in thick FGM plates. Some numerical solution of finite element method (FEM) are obtained. In 2019, Alaimo et al. [7] used the analytical procedure of Navier to investigate the frequency of composite plates embedding viscoelastic layers. Some numerical results of FEM are obtained. In 2019, Safaei et al. [8] used the mesh-free method and HSDT to investigate the frequency of FGM carbon nanotube (CNT) plate under thermo-mechanical loads. Some numerical results of dynamic behaviors are obtained. In 2019, Sun and Wei [9] used the singular boundary method (SBM) to investigate the frequency of thin elastic plates. Some numerical results of harmonic behaviors are obtained. In 2019, Vinyas et al. [10] used the HSDT of displacements to investigate the frequency of three-phase smart magneto-electro-elastic (TPS-MEE) composite plates. Some numerical results of FEM are obtained. In 2017, Rezaei et al. [11] investigated the non-dimensional frequency of

* Corresponding author. E-mail address: cchong@hust.edu.tw

Tel.: +886-919037599; Fax: +886-4-24961187

FGM plates with porosities by using linear model of displacements with analytical method. Some numerical results of non-dimensional frequencies are obtained. In 2017, Yao et al. [12] used von Karman large deformation theory and Hooke law to investigate the frequency responses of the bistable piezoelectric plate. Some numerical results of frequencies are obtained. Jha et al. investigated the numerical solutions of thick FGM with the higher order shear/shear-normal deformations theories (HOSTs/HOSNTs) in 2013, the numerical frequency solutions for free vibration of simply supported FGM plates are obtained [13]. In 2017, Duc et al. [14] used the FSDT displacement method to present the analytical solutions for static response and free vibration of carbon nanotube reinforced composite (CNTRC) FGM plates.

Several numerical investigations have been studied in the thick and thin FGMs. Hong [15] used the nonlinear model TSDT to obtain the vibration solutions for the thermal stress and deflection of the thick FGM plates in 2019. It would be interesting to study the non-dimensional and dimensional natural frequency containing the c_1 displacement term in the TSDT displacement model and calculated values of shear correction for the thick FGM plates under free vibration. Length to thickness ratio, temperature of environment and power law index of FGM three parametric effects on the non-dimensional and dimensional natural frequency of thick FGM plates are also studied.

2. Procedure of Formulations

The typically two-material plates respectively in constituent material 1 and constituent material 2 of FGMs are shown in Fig. 1 with thickness h_1 and h_2 are considered for the derivation of formulation under the thermal influence of environment. Usually, power-law type of materials function are selected to study the numerical solutions for the two-material. These standard forms of properties e.g. Young's modulus of FGM E_{fgm} can be denoted by $E_{fgm} = (E_2-E_1)[(z+h^*/2)/h^*]^{Rn}$, in which R_n is power index, E_1 and E_2 are Young's modulus of constituent material 1 and 2, respectively, for the other properties can be simplified into the mean expressions e.g. Poisson's ratios of FGM is $v_{fgm} = (v_1+v_2)/2$, in which v_1 and v_2 are Poisson's ratios of constituent material 1 and 2, respectively [16]. Also the constituent material properties P_i are denoted and found in the variation of temperature T of environment i.e. $P_i = P_0(P_{-1}T^{-1}+1+P_1T+P_2T^2+P_3T^3)$, in which P_0, P_{-1}, P_1, P_2 and P_3 are temperature coefficients. Displacements in thick plates with variables u, v and w of FGM are in dependent of time. These displacements can be denoted and assumed in the additional nonlinear coefficient c_1 term for $c_1 = 4/[3(h^*)^2]$ presented in TSDT mode [17], where h^* is the summation of two-material thickness.
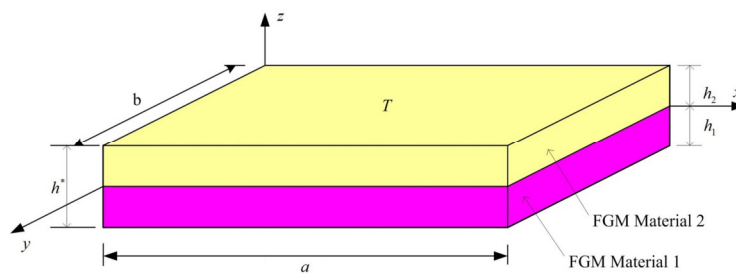
Fig. 1 Two-material FGM plate under thermal environment

The nonlinear Reddy's TSDT displacement field, strain-displacement relations and dynamic equilibrium differential equations of motion governing the FGM plates under consideration of formulations can be referred to the published paper in 2019 by Hong [15]. The inter-laminar stresses within thick FGM plate under the influence of temperature difference ΔT for the kth constituent layer can be derived and given [18-19]. The TSDT term of displacement modes in thick FGM plate contained in the dynamic equilibrium equations can be derived and given [20] with k^{th} constituent ply density $\rho^{(k)}$ integration parameters I_i, J_i and K_2, in the subscript $i = 0, 1, 2,\ldots, 6$.

Von Karman type of strain-displacement relation equations can be derived and used with displacements u^0 and v^0 are in the axes direction x and y respectively, with transverse displacement w is in the axis direction z within the middle plate of thick FGM, also with the shear rotations Ψ_x and Ψ_y are in the x and y direction of axes respectively. By substituting stress and

strain-displacement equations into dynamic equations of motion, thus the dynamic differential equations of equilibrium contained TSDT terms of thick FGM plates can be obtained in matrix forms in terms of partial derivatives of displacements, shear rotations, mechanical loads (p_1 and p_2 are external loads in axes direction x and y respectively, q is pressure load), thermal loads and inertia terms. These calculated correction values of shear coefficient $k_{\alpha h}$ are typically only in functions of parameters T, R_n and h^* [15]. Stiffness parameters are integrated and given as follows.

$$(A_{i^s j^s}, B_{i^s j^s}, D_{i^s j^s}, E_{i^s j^s}, F_{i^s j^s}, H_{i^s j^s}) = \int_{-h^*/2}^{h^*/2} \overline{Q}_{i^s j^s} (1, z, z^2, z^3, z^4, z^6) dz \tag{1}$$

$$(A_{i^* j^*}, B_{i^* j^*}, D_{i^* j^*}, E_{i^* j^*}, F_{i^* j^*}, H_{i^* j^*}) = \int_{-h^*/2}^{h^*/2} k_\alpha \overline{Q}_{i^* j^*} (1, z, z^2, z^3, z^4, z^5) dz \tag{2}$$

where $\overline{Q}_{i^s j^s}$ and $\overline{Q}_{i^* j^*}$ are transformed reduced stiffness of FGM can be simplified in 2007 by Shen [21], in which $i^s, j^s = 1, 2, 6$ and $i^*, j^* = 4, 5$.

3. Numerical Results and Discussion

The two-material FGM thick plates with same direction of constituents are selected to investigate the non-dimensional and dimensional frequency of numerical results under free vibration without thermal forces, distributed forces and pressure forces ($\Delta T = 0$, $p_1 = p_2 = 0$, $q = 0$). The dimensional frequency ω_{mn} (the subscripts m and n are mode shape numbers in the x and y direction of axes) can be simplified ($I_1 = I_3 = J_1 = 0$, $B_{ij} = E_{ij} = 0$, $D_{16} = D_{26} = A_{16} = A_{26} = 0$ and $A_{45} = D_{45} = F_{45} = 0$) and derived for the following displacements and shear rotations in simply supported boundary equations,

$$u^0 = a_{mn} cos(m\pi x / a) sin(n\pi y / b) sin(\omega_{mn} t) \tag{3}$$

$$v^0 = b_{mn} sin(m\pi x / a) cos(n\pi y / b) sin(\omega_{mn} t) \tag{4}$$

$$w = c_{mn} sin(m\pi x / a) sin(n\pi y / b) sin(\omega_{mn} t) \tag{5}$$

$$\psi_x = d_{mn} cos(m\pi x / a) sin(n\pi y / b) sin(\omega_{mn} t) \tag{6}$$

$$\psi_y = e_{mn} sin(m\pi x / a) cos(n\pi y / b) sin(\omega_{mn} t) \tag{7}$$

in which a_{mn}, b_{mn}, c_{mn}, d_{mn}, and e_{mn} are amplitudes, t is the time, a is the length and b is the width of thick FGM plates.

The major difference in the present free vibration work of simply homogeneous equation with respect to fully homogeneous equation is the calculated simplification in the matrix element terms. After Eqs. (3)-(7) have been substituted into equations of equilibrium with no external loads ($f_1 = f_2 = ... = f_5 = 0$), and by conveniently assuming that matrix element terms $FH_{13} = FH_{14} = FH_{15} = FH_{23} = FH_{24} = FH_{25} = 0$ and $I_3 = J_1 = I_6 = J_4 = 0$ in the fully homogeneous equation, thus the simply homogeneous equation for the dimensional frequency ω_{mn} contained the c_1 terms of TSDT can be obtained as follows [15].

$$\begin{bmatrix} FH_{11} - \lambda_{mn} & FH_{12} & 0 & 0 & 0 \\ FH_{12} & FH_{22} - \lambda_{mn} & 0 & 0 & 0 \\ 0 & 0 & FH_{33} - \lambda_{mn} & FH_{34} & FH_{35} \\ 0 & 0 & FH_{34} & FH_{44} - \dfrac{K_2}{I_0}\lambda_{mn} & FH_{45} \\ 0 & 0 & FH_{35} & FH_{45} & FH_{55} - \dfrac{K_2}{I_0}\lambda_{mn} \end{bmatrix} \begin{Bmatrix} a_{mn} \\ b_{mn} \\ c_{mn} \\ d_{mn} \\ e_{mn} \end{Bmatrix} = \begin{Bmatrix} 0 \\ 0 \\ 0 \\ 0 \\ 0 \end{Bmatrix} \tag{8a}$$

where

$$\lambda_{mn} = I_0 \omega_{mn}^2 \tag{8b}$$

$$FH_{11} = A_{11}(m\pi/a)^2 + A_{66}(n\pi/b)^2 \tag{8c}$$

$$FH_{12} = (A_{12} + A_{66})(m\pi/a)(n\pi/b) \tag{8d}$$

$$FH_{22} = A_{66}(m\pi/a)^2 + A_{22}(n\pi/b)^2 \tag{8e}$$

$$FH_{33} = A_{55}(m\pi/a)^2 + A_{44}(n\pi/b)^2 + c_1^2 H_{11}(m\pi/a)^4 + (2c_1^2 + 4c_1^2 H_{66})(m\pi/a)^2(n\pi/b)^2$$
$$+ c^2 H_{22}(n\pi/b)^4 - 3c_1(2D_{55} - 3c_1 F_{55})(m\pi/a)^2 - 3c_1(2D_{44} - 3c_1 F_{44})(n\pi/b)^2 \tag{8f}$$

In the derivation of mathematics, the algebraic determinant of Eq. (8a) could be presented in the following equation in terms of λ_{mn}, thus the ω_{mn} can be calculated.

$$A(1)\lambda_{mn}^5 + A(2)\lambda_{mn}^4 + A(3)\lambda_{mn}^3 + A(4)\lambda_{mn}^2 + A(5)\lambda_{mn} + A(6) = 0 \tag{9a}$$

where

$$A(1) = -sd \tag{9b}$$

$$A(2) = (FH_{11} + FH_{22})sd + sc \tag{9c}$$

$$A(3) = -[(FH_{11}FH_{22} - FH_{12}FH_{12})sd + (FH_{11} + FH_{12})sc + sb] \tag{9d}$$

$$A(4) = (FH_{11}FH_{22} - FH_{12}FH_{12})sc + (FH_{11} + FH_{22})sb + sa \tag{9e}$$

$$A(5) = -[(FH_{11}FH_{22} - FH_{12}FH_{12})sb + (FH_{11} + FH_{22})sa] \tag{9f}$$

$$A(6) = (FH_{11}FH_{22} - FH_{12}FH_{12})sa \tag{9g}$$

in which

$$sd = (K_2/I_0)^2 \tag{9h}$$

$$sc = FH_{33} sd + FH_{44}K_2/I_0 \tag{9i}$$

$$sb = (FH_{33}FH_{55} + FH_{44}FH_{55} + FH_{33}FH_{44} - FH_{35}FH_{35} - FH_{34}FH_{34})K_2/I_0 - FH_{45}FH_{45} \tag{9j}$$

$$sa = FH_{33}FH_{44}FH_{55} + FH_{44}FH_{34}FH_{35} + FH_{35}FH_{34}FH_{45} - FH_{35}FH_{35}FH_{44} - FH_{34}FH_{34}FH_{55}$$
$$- FH_{45}FH_{45}FH_{33} \tag{9k}$$

A numerical method used to calculate and solve the polynomial Eq. (9a) in terms of fifth-order of λ_{mn}, thus the natural frequency ω_{mn} can be determined. A FORTRAN program coded in the algorithm of Newton's method by Conte and de Boor in 1980 [22] is used to find the solution of Eq. (9a). The accuracy of tolerance is 1e-06 and used in the program to meet the condition of convergence then find the root of Eq. (9a). The composited FGM two-material SUS304/Si_3N_4 is implemented for the computation results under temperature of environment T. The material 1 SUS304 (stainless steel) is located at lower

position, the material 2 Si_3N_4 (silicon nitride) is located at upper position of the FGM thickness, respectively. In the preliminary and fundamental calculations, it did not consider the c_1 effect of TSDT onto the derivative of shear coefficient k_α. For example $a/b = 1$, $h_1 = h_2$, $h^* = 0.12mm$-$12mm$, the k_α values under $T = 300K$, $600K$ and $1000K$ are shown in Table 1(a), Table 1(b) and Table 1(c), respectively. When the values of k_α are calculated under the condition of cases only for the corresponding T, R_n and h^*, then they are used in getting results for Figs. 2-5.

Table 1(a) Varied k_α vs. R_n and h^* under $T = 300K$

$c_1(1/mm^2)$	$h^*(mm)$	k_α						
		R_n: 0.1	0.2	0.5	1	2	5	10
92.592598	0.12	0.098323	0.127625	0.266187	0.638005	1.007910	0.932667	0.843506
0.925925	1.2	0.079956	0.084882	0.102678	0.138574	0.217517	0.396486	0.492255
0.231481	2.4	0.075063	0.074789	0.074832	0.074112	0.064424	0.021065	0.001152
0.037037	6	0.069011	0.063127	0.048652	0.030937	0.010870	0.000220	0.000000
0.009259	12	0.064733	0.055449	0.034895	0.015697	0.002738	0.000006	0.000000

Table 1(b) Varied k_α vs. R_n and h^* under $T = 600K$

$c_1(1/mm^2)$	$h^*(mm)$	k_α						
		R_n: 0.1	0.2	0.5	1	2	5	10
92.592598	0.12	0.085699	0.111597	0.236756	0.596251	0.995481	0.923808	0.834206
0.925925	1.2	0.069478	0.073722	0.089181	0.120708	0.191371	0.359433	0.456324
0.231481	2.4	0.065173	0.064854	0.064737	0.063996	0.055506	0.018026	0.000982
0.037037	6	0.059859	0.054641	0.041932	0.026560	0.009297	0.000188	0.000000
0.009259	12	0.056109	0.047937	0.030016	0.012979	0.002340	0.000005	0.000000

Table 1(c) Varied k_α vs. R_n and h^* under $T = 1000K$

$c_1(1/mm^2)$	$h^*(mm)$	k_α						
		R_n: 0.1	0.2	0.5	1	2	5	10
92.592598	0.12	0.071316	0.091135	0.192482	0.562116	1.236624	1.094820	0.917769
0.925925	1.2	0.057519	0.059382	0.067907	0.088108	0.137812	0.270674	0.355043
0.231481	2.4	0.053882	0.052072	0.048781	0.045488	0.037321	0.011122	0.000565
0.037037	6	0.049404	0.043712	0.031294	0.018557	0.006113	0.000115	0.000000
0.009259	12	0.046254	0.038257	0.022289	0.009340	0.001533	0.000003	0.000000

The non-dimensional frequency parameters f^*, ω^*, Ω in terms of fundamental dimensional frequency ω_{11} with mode shape numbers in the subscripts $m = n = 1$ are used for SUS304/Si_3N_4 thick plate under free vibration and given as follows,

$$f^* = \omega_{11}h^*\sqrt{\rho_2 / E_2} \tag{10}$$

$$\omega^* = (\omega_{11}b^2 / \pi^2)\sqrt{I_s / D_s} \tag{11}$$

$$\Omega = (\omega_{11}a^2 / h^*)\sqrt{\rho_1(1-\nu_1^2) / E_1} \tag{12}$$

$$I_s = \int_{-h^*/2}^{h^*/2} \rho_1 dz \tag{13}$$

$$D_s = \int_{-h^*/2}^{h^*/2} \overline{Q}_1 z^2 dz \tag{14}$$

$$\overline{Q}_1 = E_1 / (1-\nu_1^2) \tag{15}$$

in which ω_{11} is the fundamental dimensional frequency, ρ_2 and ρ_1 are the density of FGM material 2 and material 1, respectively. In the Tables 2-4, the present results of non-dimensional f^*, ω^* and Ω are compared with available published paper. In Table 2, the present results of f^* vs. h^* are shown for $a/h^* = 10$, $300K$, k_α and c_1 values, we found $f^* = 0.080832$ at $h^* = 900mm$,

$R_n = 0.5$ is in close to $f^* = 0.0839$ for Al/ZrO$_2$ by Jha et al. in 2013 [13] with HOSNT12 in which 12 degrees of freedom considered for the model. In Table 3, the present results of ω^* vs. h^* are shown for $a/h^* =10$, $300K$, k_α and c_1 values, we found $\omega^* = 4.094445$ at $h^* = 600$mm, $R_n = 2$ is in close to $\omega^* = 4.1165$ with $h^* = 200$mm forced vibration by Kim in 2005 [23].

Table 2 Comparison of non-dimensional f^*

$c_1(1/mm^2)$	h^*(mm)	f^*			
		Present results, $a/h^* = 10$, $T = 300K$, varied k_α, for SUS304/Si$_3$N$_4$			Jha et al. 2013, for Al/ZrO$_2$, $R_n = 0.5$
		$R_n = 0.5$	$R_n = 1$	$R_n = 2$	
0.925925	1.2	0.003713	0.002326	0.002412	-
0.333333	2	0.008001	0.004982	0.005163	-
0.000033	200	0.017724	0.017726	0.017708	-
0.000014	300	0.026743	0.026744	0.026727	-
0.000003	600	0.053789	0.053789	0.053773	-
0.000001	900	0.080832	0.080832	0.080816	0.0839

Table 3 Comparison of non-dimensional ω^*

$c_1(1/mm^2)$	h^*(mm)	ω^*			Kim 2005, Forced vibration, $h^* = 200$mm, $R_n = 2$	Duc et al. 2017 CNTRC, FSDT
		Present results, $a/h^* = 10$, $T = 300K$, varied k_α				
		R_n: 0.5	1	2		
0.925925	1.2	0.282727	0.177156	0.183727	-	-
0.333333	2	0.609222	0.379389	0.393123	-	-
0.000033	200	1.349598	1.349716	1.348404	-	-
0.000014	300	2.036305	2.036380	2.035098	-	-
0.000003	600	4.095676	4.095697	4.094445	4.1165	3.99244 (UD)
0.000001	900	6.154796	6.154793	6.153549	-	-

Also, compare the present results with the analytical FSDT results of uniform distribution (UD) in CNTRC FGM plates by Duc et al. in 2017 [14]. In Table 4, the present results of Ω vs. h^* are shown for $a/h^* = 10$, $700K$, k_α and c_1 values, we found $\Omega = 5.1314993$ at $h^* = 250$mm, $R_n = 1$ is in close to $\Omega = 5.359$ with forced vibration under temperature rise ($\Delta T = 400K$) by Ungbhakorn & Wattanasakulpong in 2013 [24].

Table 4 Non-dimensional Ω comparison for SUS304/Si$_3$N$_4$

$c_1(1/mm^2)$	h^*(mm)	Ω			Ungbhakorn & Wattanasakulpong 2013, $R_n = 1$
		Present results, $a/h^* = 10$, $T = 700K$, varied k_α			
		R_n: 0.5	1	2	
0.925925	1.2	0.548323	0.568358	0.983723	-
0.333333	2	1.966345	1.217748	1.266043	-
0.000033	200	4.089171	4.089357	4.084728	-
0.000021	250	5.131368	5.131493	5.126937	5.359
0.000014	300	6.173302	6.173382	6.168875	-

The dimensional ω_{mn} (unit 1/s) under no temperature difference ($\triangle T = 0$) of two directional mode in the subscripts m, n are investigated. In Fig. 2, the present results of ω_{1n} vs. R_n are shown for $a/h^* = 5$ and 10, respectively for $T = 300K$, k_α and c_1 values. For the cases of $R_n = 0.5$, 1 and 10, the present results of ω_{1n} are oscillating and converging to nearly 0.005/s with n (in the subscript n = 1-9). The greatest value of $\omega_{11} = 0.054676$/s is found, then decreasing to value $\omega_{19} = 0.005694$/s for $a/h^* = 5$, $R_n = 10$. The greatest value of $\omega_{11} = 0.067990$/s is found, then decreasing to value $\omega_{19} = 0.005715$/s for $a/h^* = 10$, $R_n = 10$. When $n = 9$, the frequencies are almost meeting at a point, e.g. $\omega_{19} = 0.005694$/s for $a/h^* = 5$, $Rn = 0.5$, 1 and 10, also $\omega_{19} = 0.005715$/s for $a/h^* = 10$, $Rn = 0.5$ and 1, but not for $Rn = 10$. The frequencies would be meeting closely at a point for all the value of Rn when the values of n are greater more than 9.

(a) $a/h^* = 5$ (b) $a/h^* = 10$
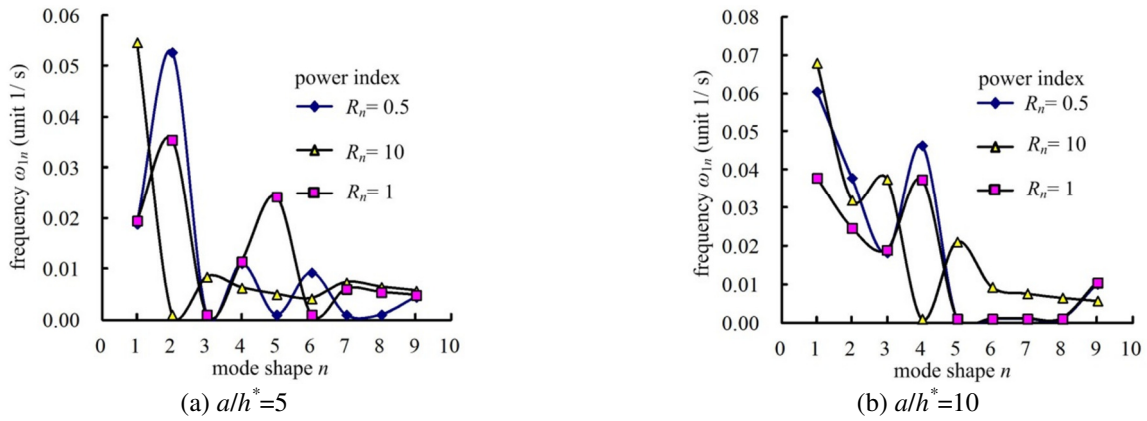
Fig. 2 ω_{1n} (unit 1/s) vs. R_n

In Fig. 3, the present results of ω_{1n} vs. T are shown for $a/h^* = 5$ and 10, respectively for $R_n = 0.5$, k_a and c_1 values. Generally the values of ω_{1n} are oscillating and converging to nearly 0.005/s with n (in the subscript $n = 1$-9) for $T = 300K$, $600K$ and $1000K$. The greatest value of $\omega_{12} = 0.059699$/s is found, then decreasing to value $\omega_{19} = 0.001000$/s for $a/h^* = 5$, $T = 600K$. The greatest value of $\omega_{11} = 0.060500$/s is found, then decreasing to value $\omega_{19} = 0.010078$/s for $a/h^* = 10$, $T = 600K$. When $n = 9$, the frequencies are almost meeting at a point, e.g. $\omega_{19} = 0.001000$/s for $a/h^* = 5$, $T = 600K$ and $1000K$, but not for $T = 300K$, also $\omega_{19} = 0.010078$/s for $a/h^* = 10$, $T = 300K$, $600K$ and $1000K$. The frequencies would be meeting closely at a point for all the value of T when the values of n are greater more than 9.

(a) $a/h^* = 5$ (b) $a/h^* = 10$
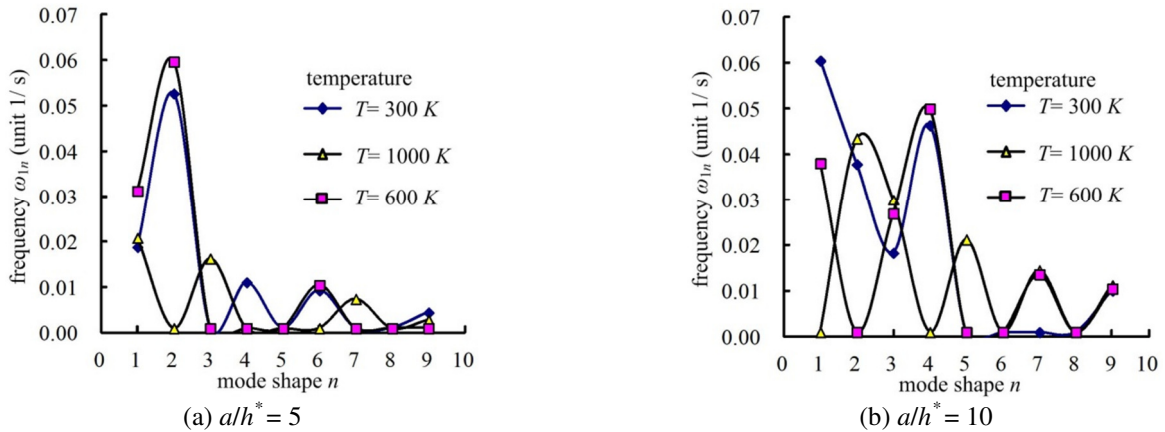
Fig. 3 ω_{1n} (unit 1/s) vs. T

The influence of gradation of material properties e.g. Rn values and thermal effect e.g. T values used on the vibration can be described in Figs. 2-3 as follows. The present results of ω_{1n} are oscillating and converging with the Rn values. Also the present results of ω_{1n} are oscillating and converging with the T values. The trend of the curves will not change for the non-dimensional and dimensional frequencies.
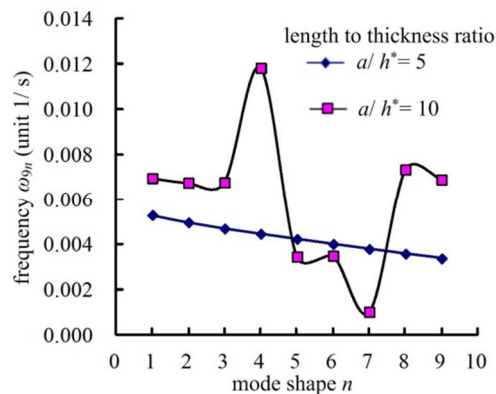
Fig. 4 ω_{9n} (unit 1/s) vs. n

In Fig. 4, the present results of ω_{9n} vs. n are shown for $a/h^* = 5$ and 10, respectively for $T = 300K$, $R_n = 0.5$, k_α and c_1 values. In general, the values ω_{9n} are oscillating with n (in the subscript $n = 1$-9) for $a/h^* = 10$. The values ω_{9n} are linearly decreasing with n for $a/h^* = 5$. The greatest value of $\omega_{94} = 0.011816$/s is found, then decreasing to value $\omega_{97} = 0.001000$/s for $a/h^* = 10$. The greatest value of $\omega_{91} = 0.005274$/s is found, then decreasing to value $\omega_{99} = 0.003356$/s for $a/h^* = 5$.

For TSDT coefficient $c_1 = 0$, the results can be added as shown in Fig. 5 and recently can't be compared with pretty rare published data. In Fig. 5(a), the present results of ω_{1n} vs. R_n are shown for $a/h^* = 5$, $T = 300K$, varied k_α and $c_1 = 0$. The values of ω_{1n} are decreasing smoothly with $n = 1$-6, but have a jump at $n = 7$, then also decreasing smoothly with $n = 8$-9. The greatest value of ω_{1n} is 0.019021/s for $R_n = 10$ at $n = 1$, it is almost three times smaller than that 0.054676/s in the nonzero of c_1 case. In Fig. 5(b), the present results of ω_{1n} vs. T are shown for $a/h^* = 5$, $R_n = 0.5$, varied k_α and $c_1 = 0$. The values of ω_{1n} are decreasing smoothly with $n = 1$-6 for $T = 300K$ and $600K$, but have a jump at $n = 7$, then also decreasing smoothly with $n = 8$-9. The values of ω_{1n} are decreasing smoothly with $n = 1$-5 for $T = 1000K$, but have a jump at $n = 6$, then also decreasing smoothly with $n = 7$-9. The greatest value of ω_{1n} is 0.0188063/s for $T = 1000K$ at $n = 1$, it is a little smaller than that 0.020803/s in the nonzero of c_1 case. In Fig. 5(c), the present results of ω_{9n} vs. n are shown for $a/h^* = 5$, $T = 300K$, $R_n = 0.5$, varied k_α and $c_1 = 0$. The values of ω_{9n} are decreasing linearly with $n = 1$-9. The greatest value of ω_{9n} is 0.007045/s at $n = 1$, it is a little greater than that 0.005274/s in the nonzero of c_1 case. The varied k_α and c_1 value of TSDT have great effect on the values of natural frequencies.
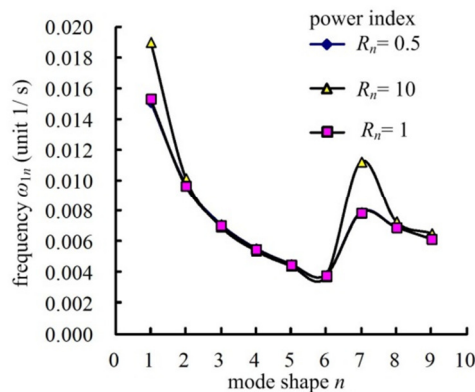
(a) ω_{1n} (unit 1/s) vs. R_n for $T = 300K$
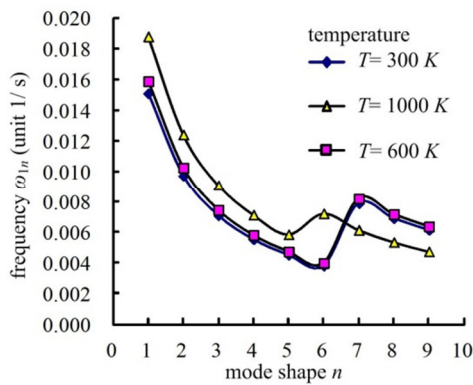
(b) ω_{1n} (unit 1/s) vs. T for $R_n = 0.5$
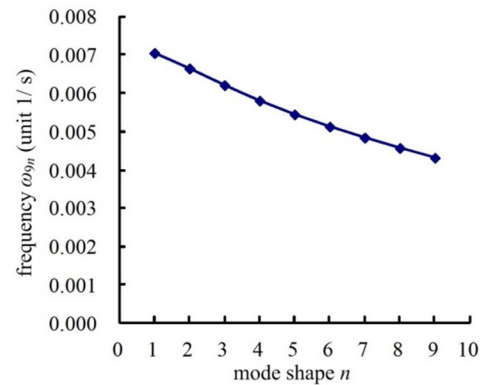
(c) ω_{9n} (unit 1/s) vs. n for $T = 300K$, $R_n = 0.5$

Fig. 5 $c_1 = 0$ for $a/h^* = 5$ and varied k_α

Similar way for keeping $n = 1$ and varying m from 1 to 9, the ω_{m1} can also be plotted and results can be included and discussed for varied k_α and c_1 values as shown in Figs. 6-7. In Fig. 6, the present results of ω_{m1} vs. R_n are shown for $a/h^* = 5$ and 10, respectively for $T = 300K$, k_α and c_1 values. The cases of $R_n = 0.5$, 1 and 10 in the present results of ω_{m1} are small oscillating and converging to nearly 0.005/s with m (in the subscript $m = 1$-9). The greatest value of $\omega_{11} = 0.054676$/s is found, then decreasing to value $\omega_{91} = 0.005969$/s for $a/h^* = 5$, $R_n = 10$. The greatest value of $\omega_{11} = 0.067990$/s is found, then decreasing to value $\omega_{91} = 0.004257$/s for $a/h^* = 10$, $R_n = 10$. When $m = 9$, the frequencies are almost meeting at a point, e.g. $\omega_{91} = 0.005969$/s

for $a/h^* = 5$, $Rn = 0.5$, 1 and 10, also $\omega_{91} = 0.006950$/s for $a/h^* = 10$, $Rn = 0.5$ and 1, but not for $Rn = 10$. The frequencies would be meeting closely at a point for all the value of Rn when the values of m are greater more than 9.

In Fig. 7, the present results of ω_{m1} vs. T are shown for $a/h^* = 5$ and 10, respectively for $R_n = 0.5$, k_α and c_1 values. The cases of $T = 300K$, $600K$ and $1000K$ in the present results of ω_{m1} are small oscillating and converging to nearly 0.005/s with m (in the subscript $m = 1$-9). The greatest value of $\omega_{11} = 0.031320$/s is found, then decreasing to value $\omega_{91} = 0.005513$/s for $a/h^* = 5$, $T = 600K$. The greatest value of $\omega_{11} = 0.098299$/s is found, then decreasing to value $\omega_{91} = 0.007040$/s for $a/h^* = 10$, $T = 1000K$. When $m = 9$, the frequencies are almost meeting at a point, e.g. $\omega_{91} = 0.005513$/s for $a/h^* = 5$, $T = 300K$ and $600K$, but not for $T = 1000K$, also $\omega_{91} = 0.007040$/s for $a/h^* = 10$, $T = 300K$, $600K$ and $1000K$. The frequencies would be meeting closely at a point for all the value of T when the values of m are greater more than 9.

(a) $a/h^* = 5$ (b) $a/h^* = 10$

Fig. 6 ω_{m1} (unit 1/s) vs. R_n

(a) $a/h^* = 5$ (b) $a/h^* = 10$
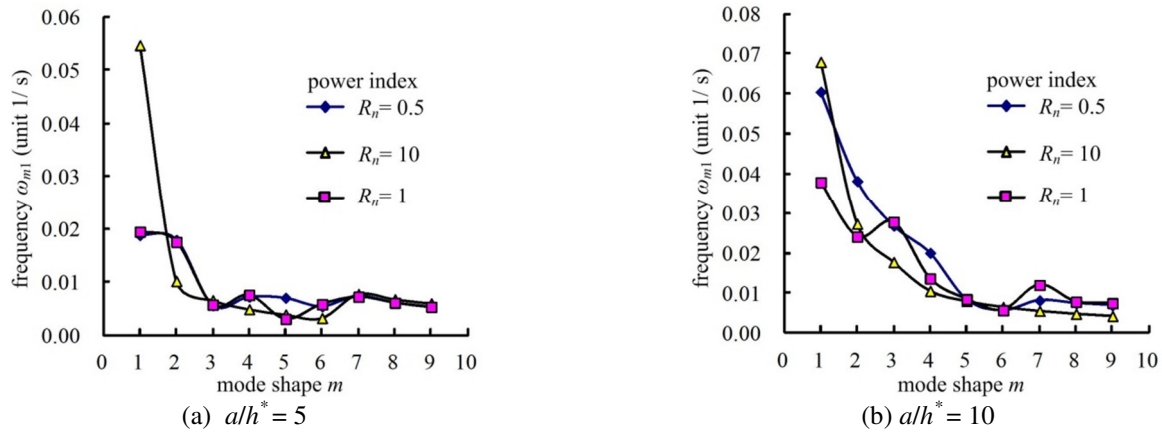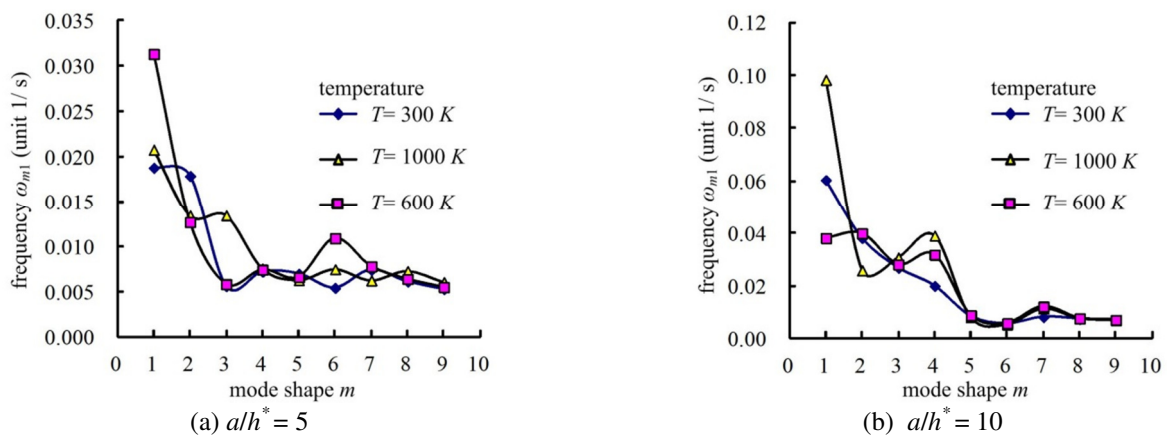
Fig. 7 ω_{m1} (unit 1/s) vs. T

The results of non-dimensional and dimensional natural frequency are obtained in free vibration of two-material thick FGM plates with power law index by considering the TSDT model, varied shear coefficient and temperature of environment. Some of the present results of non-dimensional f^*, ω^* and Ω are compared with available published paper and found in close data. It is fundamental to study the effects of varied shear coefficient values and additional c_1 displacement term in nonlinear coefficient of TSDT on the frequency calculations under free vibration. The varied k_α and c_1 value of TSDT have great effect on the values of natural frequencies. For the cases of $R_n = 0.5$, 1 and 10, the present results ω_{1n} are oscillating and converging to nearly 0.005/s with n (in the subscript $n = 1$-9). For the cases of $T = 300K$, $600K$ and $1000K$, the present results ω_{1n} are oscillating and converging to nearly 0.005/s with n (in the subscript $n = 1$-9). Similar way for keeping $n = 1$ and varying m from 1 to 9, the cases of $R_n = 0.5$, 1 and 10 in the results of ω_{m1} are small oscillating and converging to nearly 0.005/s with m (in the subscript $m = 1$-9), the cases of $T = 300K$, $600K$ and $1000K$ in the results of ω_{m1} are small oscillating and converging to nearly 0.005/s with m (in the subscript $m = 1$-9).

4. Conclusions

The natural frequency of free vibration in two-material thick FGM plates are great effected by power law index, the TSDT model, varied shear coefficient and temperature of environment. It is fundamental and new to study the additional effect of nonlinear displacement TSDT c_1 term on the frequency for two-material thick FGM plates. The present natural frequency results are oscillating and converging with respect to mode shapes by simultaneously including x and y directions. These natural frequency data of free vibration can provide a base reference and used further in the thermal vibration study in the future.

Nomenclature

h_1	Thickness of constituent material 1
h_2	Thickness of constituent material 2
h^*	Summation of two-material thickness
a	Length of thick FGM plates
b	Width of thick FGM plates
x	x direction of Cartesian axes
y	y direction of Cartesian axes
z	z direction of Cartesian axes
T	Temperature of environment
R_n	Power index in power-law type of FGM materials function
E_{fgm}	Young's modulus of FGM
E_1	Young's modulus of constituent material 1
E_2	Young's modulus of constituent material 2
v_{fgm}	Poisson's ratios of FGM
v_1	Poisson's ratios of constituent material 1
v_2	Poisson's ratios of constituent material 2
ρ_1	Density of constituent material 1
ρ_2	Density of constituent material 2
P_i	Constituent material properties
P_0, P_{-1}, P_1, P_2 and P_3	Temperature coefficients of constituent materials
u, v and w	Displacements in x, y and z directions of Cartesian axes
u^0 and v^0	Displacements in the axis directions x and y within the middle plate of thick FGM
c_1	Nonlinear Reddy's TSDT displacement field $c_1 = 4/[3(h^*)^2]$
ΔT	Temperature difference
k^{th}	k^{th} constituent layer
$\rho^{(k)}$	k^{th} constituent ply density
I_i, J_i and K_2	Density $\rho^{(k)}$ integration parameters, in the subscript $I = 0, 1, 2,…, 6$
Ψ_x and Ψ_y	Shear rotations in the x and y direction of axes
p_1 and p_2	External loads in axes direction x and y
q	Pressure load
k_α	Shear coefficient
$\bar{Q}_{i^s j^s}$ and $\bar{Q}_{i^* j^*}$	Transformed reduced stiffness of FGM with i^s, $j^s = 1, 2, 6$ and $i^*, j^* = 4, 5$
ω_{mn}	Dimensional frequency with the subscripts m and n are mode shape numbers in the x and y direction of axes
ω_{11}	Fundamental dimensional frequency with $m = n = 1$
f^*, ω^*, Ω	Non-dimensional frequency parameters
t	Time
$f_1, f_2,…, f_5$	External loads
λ_{mn}	Frequencies parameter in $\lambda_{mn} = I_0 \omega_{mn}^2$

Conflicts of Interest

The authors declare no conflict of interest.

References

[1] K. K. Żur, M. Arefi, J. Kim, and J. N. Reddy, "Free Vibration and Buckling Analyses of Magneto-Electro-Elastic FGM Nanoplates Based on Nonlocal Modified Higher-Order Sinusoidal Shear Deformation Theory," Composites Part B, vol. 182, 107601, February 2020.

[2] H. M. Ouakad, A. Valipour, K. K. Żur, H. M. Sedighi, and J. N. Reddy, "On the Nonlinear Vibration and Static Deflection Problems of Actuated Hybrid Nanotubes Based on the Stress-Driven Nonlocal Integral Elasticity," Mechanics of Materials, vol. 148, 103532, September 2020.

[3] A. Ghobadi, H. Golestanian, Y. T. Beni, and K. K. Żur, "On the Size-Dependent Nonlinear Thermo-Electro-Mechanical Free Vibration Analysis of Functionally Graded Flexoelectric Nano-Plate," Communications in Nonlinear Science and Numerical Simulation, in press.

[4] A. Ghobadi, Y. T. Beni, and K. K. Żur, "Porosity Distribution Effect on Stress, Electric Field and Nonlinear Vibration of Functionally Graded Nanostructures with Direct and Inverse Flexoelectric Phenomenon," Composite Structures, in press.

[5] H. Guo, T. Yang, K. K. Żur, and J. N. Reddy, "On the Flutter of Matrix Cracked Laminated Composite Plates Reinforced with Graphene Nanoplatelets," Thin-Walled Structures, vol. 158, 107161, January 2021.

[6] M. Babaei, M. H. Hajmohammad, and K. Asemi, "Natural Frequency and Dynamic Analyses of Functionally Graded Saturated Porous Annular Sector Plate and Cylindrical Panel Based on 3D Elasticity," Aerospace Science and Technology, vol. 96, 105524, January 2020.

[7] A. Alaimo, C. Orlando, and S. Valvano, "Analytical Frequency Response Solution for Composite Plates Embedding Viscoelastic Layers," Aerospace Science and Technology, vol. 92, pp. 429-445, September 2019.

[8] B. Safaei, R. Moradi-Dastjerdi, Z. Qin, and F. Chu, "Frequency-Dependent Forced Vibration Analysis of Nanocomposite Sandwich Plate under Thermo-Mechanical Loads," Composites Part B, vol. 161, pp. 44-54, March 2019.

[9] L. Sun and X. Wei, "A Frequency Domain Formulation of the Singular Boundary Method for Dynamic Analysis of Thin Elastic Plate," Engineering Analysis with Boundary Elements, vol. 98, pp. 77-87, January 2019.

[10] M. Vinyas, K. K. Sunny, D. Harursampath, T. Nguyen-Thoi, and M. A. R. Loja, "Influence of Interphase on the Multi-Physics Coupled Frequency of Three-Phase Smart Magneto-Electro-Elastic Composite Plates," Composite Structures, vol. 226, 111254, October 2019.

[11] A. S. Rezaei, A. R. Saidi, M. Abrishamdari, and M. H. Pour Mohammadi, "Natural Frequencies of Functionally Graded Plates with Porosities via a Simple Four Variable Plate Theory: An Analytical Approach," Thin-Walled Structures, vol. 120, pp. 366-377, November 2017.

[12] M. Yao, W. Hu, and W. Zhang, "Nonlinear Frequency Responses of the Bistable Piezoelectric Plate," Procedia IUTAM, vol. 22, pp. 208-215, 2017.

[13] D. K. Jha, T. Kant, and R. K. Singh, "Free Vibration Response of Functionally Graded Thick Plates with Shear and Normal Deformations Effects," Composite Structures, vol. 96, pp. 799-823, February 2013.

[14] N. D. Duc, J. Lee, T. Nguyen-Thoi, and P. T. Thang, "Static Response and Free Vibration of Functionally Graded Carbon Nanotube-Reinforced Composite Rectangular Plates Resting on Winkler–Pasternak Elastic Foundations," Aerospace Science and Technology, vol. 68, pp. 391-402, September 2017.

[15] C. C. Hong, "GDQ Computation for Thermal Vibration of Thick FGM Plates by Using Fully Homogeneous Equation and TSDT," Thin-Walled Structures, vol. 135, pp. 78-88, February 2019.

[16] S. H. Chi and Y. L. Chung, "Mechanical Behavior of Functionally Graded Material Plates Under Transverse Load, Part I: Analysis," International Journal of Solids and Structures, vol. 43, no. 13, pp. 3657-3674, June 2006.

[17] S. J. Lee, J. N. Reddy, and F. Rostam-Abadi, "Transient Analysis of Laminated Composite Plates with Embedded Smart-Material Layers," Finite Elements in Analysis and Design, vol. 40, no. 5-6, pp. 463-483, March 2004.

[18] S. J. Lee and J. N. Reddy, "Non-Linear Response of Laminated Composite Plates Under Thermomechanical Loading," International Journal of Non-Linear Mechanics, vol. 40, no. 7, pp. 971-985, September 2005.

[19] J. M. Whitney, "Structural Analysis of Laminated Anisotropic Plates," U.S.A: CRC Press, 1987.

[20] J. N. Reddy, "Energy Principles and Variational Methods in Applied Mechanics," New York: Wiley, 2017.

[21] H. S. Shen, "Nonlinear Thermal Bending Response of FGM Plates due to Heat Condition," Composites Part B: Engineering, vol. 38, pp. 201-215, 2007.

[22] S. D. Conte and C. de Boor, "Elementary Numerical Analysis, an Algorithmic Approach," 3rd ed. U.S.A.: McGraw-Hill Book Company, 1980.

[23] Y. W. Kim, "Temperature Dependent Vibration Analysis of Functionally Graded Rectangular Plates," Journal of Sound and Vibration, vol. 284, no. 3-5, pp. 531-549, June 2005.

[24] V. Ungbhakorn and N. Wattanasakulpong, "Thermo-Elastic Vibration Analysis of Third-Order Shear Deformable Functionally Graded Plates with Distributed Patch Mass Under Thermal Environment," Applied Acoustics, vol. 74, no. 9, pp. 1045-1059, September 2013.